Ultrasonics 116 (2021) 106483

Contents lists available at ScienceDirect

Ultrasonics

journal homepage: www.elsevier.com/locate/ultras

Numerical parametric study of Nonlinear Coda Wave Interferometry sensitivity to microcrack size in a multiple scattering medium

Guangzhi Chen [a,b,c], Yuxiang Zhang [a,b,c,*], Odile Abraham [d,*], Damien Pageot [d], Mathieu Chekroun [e], Vincent Tournat [e]

[a] Acoustic Science and Technology Laboratory, Harbin Engineering University, Harbin 150001, China
[b] Key Laboratory of Marine Information Acquisition and Security (Harbin Engineering University), Ministry of Industry and Information Technology, Harbin 150001, China
[c] College of Underwater Acoustic Engineering, Harbin Engineering University, Harbin 150001, China
[d] GERS-GeoEND, Univ Gustave Eiffel, IFSTTAR, F-44344 Bouguenais, France
[e] Laboratoire d'Acoustique de l'Université du Mans (LAUM), UMR 6613, Institut d'Acoustique - Graduate School (IA-GS), CNRS, Le Mans Université, France

ARTICLE INFO

Keywords:
Nonlinear Coda Wave Interferometry (NCWI)
Numerical modeling
Nonlinear acoustics
Spectral Element Method (SEM)

ABSTRACT

This paper reports a numerical study of the sensitivity and applicability of the Nonlinear Coda Wave Interferometry (NCWI) method in a heterogeneous material with a localized microcracked zone. We model the influence of a strong pump wave on the localized microcracked zone as a small average increase in the length of each crack. Further probing of this microcracked zone with a multiply scattered ultrasonic wave induces small changes to the coda-type signal, which are quantified with coda wave interferometry. A parametric sensitivity study of the CWI observables with respect to the changes in crack length is established via numerical simulations of the problem using a 2D spectral element method (SEM2D). The stretching of the signal, proportional to the relative variation in effective velocity, is found to be linearly proportional to the global change in crack length, while the other CWI parameter, the remnant decorrelation coefficient, is found to be quadratically proportional to the crack length change. The NCWI method is shown to be relevant for the detection of different damaged material states in complex solids. The reported numerical results are especially significant in the context of quantitative nondestructive evaluation of micro-damage level of a heterogeneous materials using nonlinear ultrasound signals.

1. Introduction

Nonlinear ultrasonic testing methods are known to exhibit a high sensitivity to the presence of microcracks or to early damage detection in complex materials [1–5], whereas conventional linear ultrasonic methods are typically less sensitive but sometimes more quantitative, such as with single cracks in homogeneous samples. Signatures of nonclassical nonlinearity, in particular, are very promising for non-destructive testing (NDT) in different domains, *e.g.*, geosciences [6,7] and medical imaging [8,9]. The elastic behavior of highly heterogeneous materials such as concrete, rock, sand, and soil exhibit strong nonlinearities, particularly nonclassical ones in the form of tapping contact acoustic nonlinearities [10–14], hysteresis in the stress–strain relation [15–18], slow dynamics, and discrete memory [2,6,19,20]. Such nonclassical nonlinearities are closely related to the presence of internal microcontacts which might result from material damage, such as microcracks [21–24].

For its advantageous sensitivity in detecting early stage damages and micro-damages, nonlinear ultrasonic NDT methods have been actively studied and reported in the last decades, e.g. harmonic generation [25,26], nonlinear resonance method [6,27,28], nonlinear modulation, acousto-elasticity, and dynamic acousto-elasticity method [29–32]. It's then pointed out that, when these methods are utilized to analyze nonlinear phenomenon that is not purely stemming from the classical potential atomic nonlinearity leading to a quadratic or cubic stress–strain relationship, they exhibits a particular sensitivity to mesoscopic features of the propagation medium such as micro-cracks or micro-contacts [33]. Compared with the effects from such nonclassical nonlinearity, ones that are from the background classical nonlinearity can be even neglected, leaving only the effects caused by the presence of microdamage/defects to be observed, which is undoubtedly of great interest for nondestructive testing applications.

* Corresponding authors.
E-mail addresses: yuxiang.zhang@hrbeu.edu.cn (Y. Zhang), odile.abraham@univ-eiffel.fr (O. Abraham).

https://doi.org/10.1016/j.ultras.2021.106483
Received 6 August 2020; Received in revised form 26 May 2021; Accepted 26 May 2021
Available online 1 June 2021

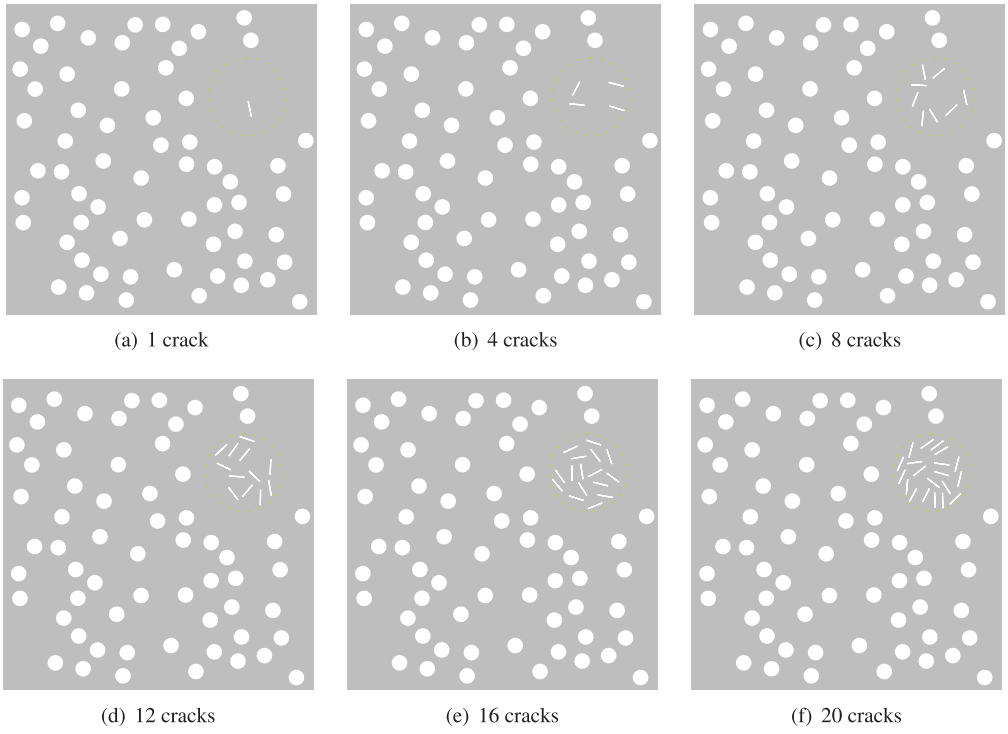

Fig. 1. Numerical configurations of damaged material with random cracks localized in a circular EDZ, centered at (155 mm, 140 mm). Each model contains a different number of cracks, ranging from 1 to 20. The matrix size is 200 mm × 200 mm. The crack size is initially set to 10 mm × 0.01 mm and their orientation is random. The source position is at (50 mm, 200 mm).

In this study, using numerical simulations, we advance the understanding of how the results of a specific nonlinear ultrasonic method depend on the presence and features of localized cracks in a highly heterogeneous medium. The method, called Nonlinear Coda Wave Interferometry (NCWI), is a combination of the nonlinear modulation method, widely studied in the context of characterizing and detecting material damage [6,34], and the coda wave interferometry [35,36], which is suitable for monitoring multiple scattered waves in complex media. A generated ultrasonic pulse is multiply scattered in a heterogeneous solid, repeatedly probes a whole region of space, and is then detected as a long-lasting signal corresponding to the summed contributions of wave trains resulting from many scattering events and arriving from many different propagation paths, a so-called coda signal. This type of complex signal is very sensitive to small changes in the propagation medium [37–39] and can be efficiently analyzed via cross-correlation with a reference signal (the basis of coda wave interferometry, or CWI) [40,41]. By further applying a lower frequency to the medium at various amplitudes (pump wave), one can monitor the induced changes to the coda signals, phase and waveform in particular, and deduce the level of related elastic nonlinearity, leading to NCWI.

This method, first applied to cracked glass samples [42], has been tested in various configurations, such as cracked mortar samples [43] and damaged concrete samples.[44] Numerical simulations in configurations related to this method have also been carried out with the spectral element method [45] in a 2D configuration, where the elastic parameters of a zone of the reverberating (or multiple-scattering) domain were slightly changed in order to extract the subsequent effects on the NCWI observables [46]. More recently, we numerically explored some of the limits of NCWI regarding the elasticity change assumed to be generated by a pump wave, the distributed damage, and the scattering role of a collection of cracks [47].

In the present article, we report results on the influence of small changes applied to a collection of cracks, and examine how these changes are manifested in the NCWI observables. Localized random arrangements of cracks, numerically modeled as thin segments exhibiting stress-free boundary conditions, are assumed to be modified, on average, due to the pump wave action: the effective length of each crack is changed by a given amount for a given pump wave amplitude. Simple dependencies of crack length change with respect to the NCWI observables are identified, and these are of potential interest for a more quantitative nondestructive evaluation of complex materials by ultrasound signals.

2. Modeling and numerical simulation

In our previous study [46], the corresponding nonclassical nonlinear phenomena was modeled in an effective manner: the influence of a strong pump wave on a localized damage was modeled by a change in the elastic properties, namely the Young's modulus and the attenuation coefficient, which were chosen to be homogeneous over an effective damaged zone (EDZ). To further advance our understanding, a considerably more realistic model is utilized in the present study: the localized damage in a heterogeneous propagation medium is materialized with a cluster of cracks that are individually modeled as high-aspect-ratio inclusions characterized by stress-free boundary conditions.

As depicted in Fig. 1, our 2D propagation medium is a 200 mm × 200 mm matrix. In a circular area centered at (155 mm, 140 mm) (top-right corner), identical cracks are placed within at random, *i.e.* at random locations with random orientations, to simulate the material damage. In this sample medium, linear heterogeneity is introduced by adding empty holes to the matrix [48]: a given number of inclusions (circular voids with a diameter of 10 mm) are randomly placed in the matrix leaving a surface filling ratio of about 12.8%. The cracks are modeled using hollow rhombi with a fixed size of 10 mm × 0.01 mm, the corresponding aspect ratio (10^3) being in line with that of cracks observed in rock materials [49]. The propagation medium is made of glass, of which mechanical properties are reported in Table 1. The area surrounding the propagation medium, including the inside of the cracks, is considered to be void to maximize the contrast of acoustic impedance, and hence the reflection coefficient, at all boundary surfaces. The damage degree is modeled by the number of cracks N_{crack}:

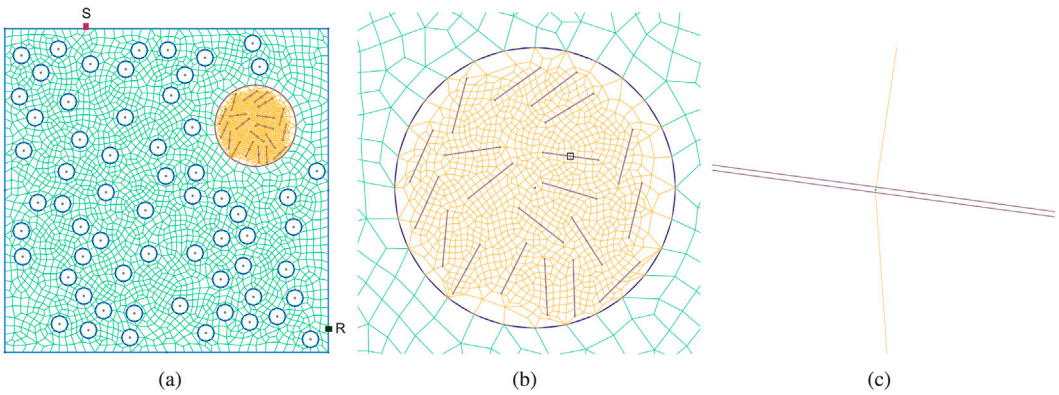

Fig. 2. An example mesh for a heterogeneous model with 20 cracks of random orientations. Each crack is modeled by one void cell, and the size of the cracks is $10\,\text{mm} \times 0.01\,\text{mm}$. The blue lines represent the contour of the matrix, the EDZ, and the cracks. The matrix size is $200\,\text{mm} \times 200\,\text{mm}$, and the circular EDZ center is located at $(155\,\text{mm}, 140\,\text{mm})$. The source position is $(50\,\text{mm}, 200\,\text{mm})$. (a) Mesh of the global configuration; (b) Magnified view of the meshed EDZ; (c) Magnified view of one crack corresponding to the square in (b).

six values ranging from 1–20 are considered in this study, as shown in Fig. 1. Five configurations of disorder are created for each damage degree with the same value of N_{crack}, *i.e.* all N_{crack} cracks are relocated and repositioned randomly. For simplification purpose, no interaction between inclusions is assumed, *i.e.*, linear or nonlinear, inclusions do not overlap.

Numerical simulations of probe wave propagation were performed using the 2D spectral element method (SEM) [45], in which wave fields are expressed in terms of high-degree Lagrangian interpolations and integral calculations are based on the Gauss–Lobatto–Legendre quadrature. The propagation medium is meshed with quadrangle cells using the GMSH software [50]. Taking into account the complexity of quad meshing, the calculation costs, and the wavelength in the working frequency range, the maximum cell size was set to be 5 mm outside the damaged zone. The damaged zone was meshed with refined cells to adapt to the size of the cracks. No meshing was applied in the inner part of the inclusions and cracks, as these are considered to be voids. A mesh example for a propagation medium containing 20 cracks is shown in Fig. 2.

To simulate the application of NCWI to the modeled propagation medium, both pump waves and probe waves are, in principle, required. The propagation of the ultrasonic probe wave was simulated directly by sending a 0.2-ms-long chirp signal with a frequency band of $[200\,\text{kHz}, 800\,\text{kHz}]$ through an acoustic point source placed at $(50\,\text{mm}, 200\,\text{mm})$ (Fig. 2-a) on the border of the domain. Synchronized with this emission, the displacement at $(200\,\text{mm}, 20\,\text{mm})$ (Fig. 2-a) over the subsequent 2.5 ms was extracted as the recorded probe signal. The presence of pump waves was accounted for, less straightforwardly, through its known impact on cracks: a small effective increase in the crack length.

Being a potential NDT method, NCWI aims for detecting damages at an early stage, which is often formed by cracks/micro-cracks that are closed or partially closed [43,44]. Assuming an elastic material and a symmetrical pump wave signal, the local stress generated is then symmetrical, i.e. the compressional and tensile stress at the same amplitude shifts periodically. In the case of an open crack, although such stress fluctuation will have its length vary continuously, but on average, its effective length over many pump wave periods remains unchanged. On the other hand, a closed crack will only respond to the tensile stress, which leads to an increase in its effective length. And a partially closed is considered as the combination of the two, its effective length will be increased under such a pump wave excitation. Therefore, due to the asymmetry in the response of cracks (closed or partially closed) to the pump wave, which could be further aggravated in the case of a certain material (e.g. concrete, whose effective stiffness in traction is only 1/3 of that in compression), its average effect will be a slight increase of crack's effective length. Assuming that the pump wave energy is homogeneously distributed over the damaged zone [51], the changes in crack's effective length $\Delta L_{crack}/L_{crack}$ were considered to be identical for all cracks. Relative to the reference state, where $\Delta L_{crack}/L_{crack} = 0$ due to the absence of the pump wave, four nonzero pump wave levels were considered, corresponding to $\Delta L_{crack}/L_{crack}$ values of 0.4%, 0.8%, 1.2%, and 1.6%, *i.e.* relatively small changes in crack length.

Probe signals recorded in medium containing four cracks and 20 cracks are shown in Fig. 3-a and 3-b, respectively. These signals exhibit typical features shared by multiple scattered waves, and are highly similar to those obtained experimentally from reverberating medium [42,52,53]. The blue signals correspond to the reference state in which the pump wave is absent ($\Delta L_{crack}/L_{crack} = 0$), while the green signals correspond to the state with the maximum pump wave level ($\Delta L_{crack}/L_{crack} = +1.6\%$). Magnified views of the same signals are presented in the lower graphs, providing details of the signals within two narrow time windows. Note that the overall change of propagation medium (geometric length of the cracks) triggered by the pump wave has only a slight effect, as no difference can be visually distinguished in the earlier time window (zoom-1). In the later time window (zoom-2), which almost exclusively contains coda waves that have been multiply scattered, the differences become more distinguishable, and such a difference can be more clearly observed in Fig. 3-b, which illustrates a more severe damage degree. This is in agreement with previous experimental results [51].

3. NCWI results

Six different damage degrees, indicated by the crack number $N_{crack} \in [1, 4, 8, 12, 16, 20]$, were studied, each containing five different disorder arrangements. In total, 30 different material configurations were numerically investigated. For each material configuration, five increasing ΔL_{crack} values were considered (assumed to be equivalent to five pump wave amplitudes), and the CWI analyses were performed using the stretching method. By comparing signals obtained with the effect of pump waves ($\Delta L_{crack} > 0$) to those obtained in the reference state ($\Delta L_{crack} = 0$) within a given time window, CWI results were obtained as the effective velocity variation θ_{coda} and the remnant decorrelation coefficient Kd. The time window for CWI analysis should be carefully selected, the sensitivity kernel of coda waves within should be stable and able to cover the probing area effectively [54]. Choosing a compromise between the analysis robustness and the calculation costs, the time window $[1.5\,\text{ms}, 2\,\text{ms}]$ was selected [46].

The obtained CWI results are plotted against $\Delta L_{crack}/L_{crack}$ in Fig. 4, where the average values and standard deviation were obtained from the five different disorder arrangements. In Fig. 4-a, from top to bottom,

Table 1
Numerical model properties used in the simulations.

Glass — properties				
Young's modulus (E) [GPa]	Poisson's ratio (ν)	Mass density (ρ) [Kg m^{-3}]	P-wave velocity (v_P) [m s^{-1}]	S-wave velocity (v_S) [m s^{-1}]
69	0.25	2500	5755	3323

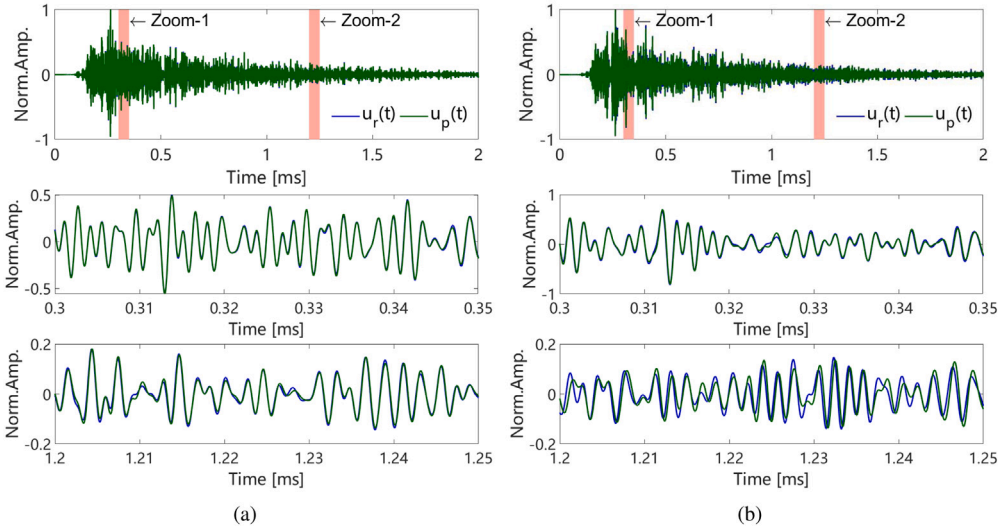

Fig. 3. Examples of temporal signals for the model with (a) four random cracks and (b) 20 random cracks. The blue lines correspond to the reference model with no change in the crack length ($\Delta L_{crack}/L_{crack} = 0$), whereas the green lines correspond to the model with an effective change in crack lengths ($\Delta L_{crack}/L_{crack} = +1.6\%$), assumed to originate from the pump wave action.

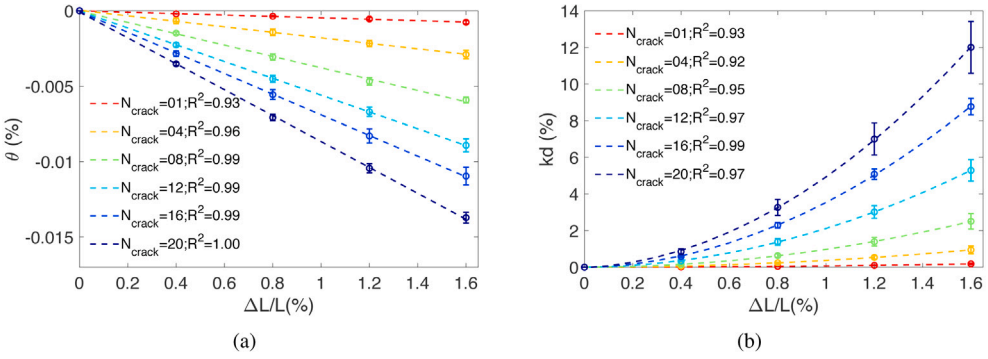

Fig. 4. CWI observables versus changes in the crack length ($\Delta L_{crack}/L_{crack}$). For each fixed number of random cracks ($N_{crack} \in [1, 4, 8, 12, 16, 20]$), five numerical models were used. (a) Relative variation in velocity θ_{coda} versus $\Delta L_{crack}/L_{crack}$; (b) Remnant decorrelation coefficient Kd versus $\Delta L_{crack}/L_{crack}$..

we plot θ_{coda} with increasing $\Delta L_{crack}/L_{crack}$ obtained for six progressively increasing damage degrees. Each circle represents the average of five θ_{coda} values obtained from five material configurations at the same damage degree and for a given $\Delta L_{crack}/L_{crack}$. The corresponding standard deviation is shown with error bars. The dashed line in Fig. 4-a shows the best-fit linear regression, with the fitting quality estimated by the coefficient of determination R^2. As the linear dependence is clear and $R^2 > 0.9$ for all cases, the linear relation connecting θ_{coda} with $\Delta L_{crack}/L_{crack}$ can be written as follows, with the slope denoted by α_θ^L:

$$\theta_{coda} = \alpha_\theta^L \cdot \left(\frac{\Delta L_{crack}}{L_{crack}} \right) \quad . \tag{1}$$

The results for Kd are plotted in Fig. 4-b in a similar manner, the only difference being that the dashed line indicates the best-fit of a quadratic regression. With the fitting quality remaining highly satisfactory, Kd is related to $\Delta L_{crack}/L_{crack}$ with a quadratic relation (Eq. (2)) in which the quadratic coefficient is denoted by α_{Kd}^L:

$$\mathrm{Kd} = \alpha_{\mathrm{Kd}}^L \cdot \left(\frac{\Delta L_{crack}}{L_{crack}} \right)^2 \quad . \tag{2}$$

As shown in Fig. 4-b, the standard deviation of Kd increases significantly as the crack density rises, which means that slightly different CWI observables are obtained from different configurations of crack disorder, and that these values differ more from one configuration to another at larger crack densities. This observation may arise from the fact that the scattering mean free path is shorter for the configurations with large crack density. The corresponding waves are consequently subjected to more scattering events, leading to a higher influence of the disorder-specific configuration. Regardless, the influence of the crack disorder configuration is much less important than the crack density on these results.

The parameters α_θ^L and α_{Kd}^L are related to the elastic nonlinearity of the propagation medium, or, in other words, to the susceptibility of the material to a pump wave. As the elastic nonlinearity stems from

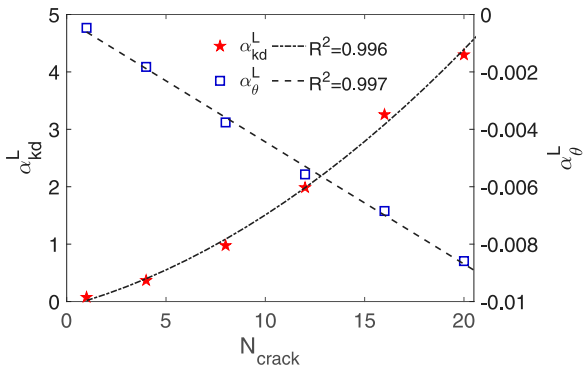

Fig. 5. Slopes of CWI observables with crack length changes versus crack density N_{crack}. For each fixed number of random cracks ($N_{crack} \in [1, 4, 8, 12, 16, 20]$), five numerical models were used. For each group of models, five crack disorder arrangements were considered in order to calculate the mean value of α^L_{Kd} (red pentagram) and α^L_{θ}(blue square), their slopes versus crack density N_{crack} are obtained with linear and quadratic regression and illustrated with dash–dot line and dashed line, respectively.

the presence of cracks, which are assumed to be identical in this study, it is interesting to plot α^L_{θ} and α^L_{Kd} versus the number of cracks N_{crack}. Fig. 5 illustrates the dependence of these parameters on the damage degree N_{crack}. As shown in Fig. 5, a linear proportionality between α^L_{θ} and N_{crack} (dashed line) has a very high fitting quality. This is consistent with previous experimental results: applying NCWI to mortar samples at different damage levels, the nonlinear parameter related to θ is reported to be linearly correlated to the damage level characterized by the size (volume) of a single penetrating macrocrack [43].

$$\begin{aligned}\theta_{coda} &= \alpha_{\theta}^{\sum L} \times \left(\sum_{N_{crack}} \frac{\Delta L_{crack}}{L_{crack}} \right) \\ &= \alpha_{\theta}^{\sum L} \times \left(\frac{\Delta L_{crack}}{L_{crack}} \times N_{crack} \right) \quad .\end{aligned} \tag{3}$$

From this empirically obtained linear dependence, the linear relationship between the effective velocity and the crack length is expressed by Eq. (3). Similarly, according to Fig. 5, a quadratic dependence between α^L_{Kd} and the crack density N_{crack} can be observed as the dash–dot line, providing a relation between the remnant decorrelation coefficient Kd and the total change in crack length:

$$\begin{aligned}\mathrm{Kd} &= \alpha_{\mathrm{Kd}}^{\sum L} \times \left(\sum_{N_{crack}} \frac{\Delta L_{crack}}{L_{crack}} \right)^2 \\ &= \alpha_{\mathrm{Kd}}^{\sum L} \times \left(\frac{\Delta L_{crack}}{L_{crack}} \times N_{crack} \right)^2 \quad .\end{aligned} \tag{4}$$

When an incident wave impinges on an obstacle in a propagation medium, it is forced to deviate from its current propagation trajectory and redistributes its energy in different directions. Such an obstacle is referred to as a scatterer, and its ability to modify the incident wave is generally quantified by its elastic scattering cross-section σ [55]. In this study, the maximum variation of crack length was 1.6% for an initial length of 10 mm, *i.e.* a maximum variation of 160 μm. For such small relative variations, a linear relationship between the scattering cross-section and the crack length can be assumed.

In a homogeneous and linear viscoelastic equivalent effective medium, the inverse quality factor Q^{-1} is determined by the average scattering cross-section $\langle \sigma^{\star} \rangle$ and the density of defects N [56]: $Q^{-1} \propto N \times \langle \sigma^{\star} \rangle$. Because it is connected to the average scattering cross-section, the inverse quality factor should be linearly related to the global length variations in the damaged material: $Q^{-1} \propto \sum \Delta L_{crack}/L_{crack}$. A quadratic relation between Kd and the change in the effective attenuation coefficient ΔQ^{-1} was reported in our previous numerical study [46]. As such, the remnant decorrelation coefficient Kd should vary quadratically with the length variations $\Delta L_{crack}/L_{crack}$. This assumption is confirmed numerically by Eq. (4), where $\mathrm{Kd} \propto (\sum \Delta L_{crack}/L_{crack})^2$. Note that this dependency also matches the earliest interpretations in this field, invoking quadratic hysteresis, as in the experiment of Zhang et al. [42]: indeed, a quadratic relation between Kd and the pump wave amplitude has been observed ($\mathrm{Kd} \propto A^2_{pump}$).

4. Case of a reverberating medium

To complete this study on the sensitivity of crack length using the NCWI method, the same parametric investigation of NCWI for crack length change was established for a homogeneous matrix with six cracking levels.

The general trends of the observables ($\theta, Kd, \alpha^L_{\theta}, \alpha^L_{\mathrm{Kd}}$) in this homogeneous reverberating medium (Figs. 6 and 7) are the same as for the highly heterogeneous medium (Figs. 4 and 5). The relations between the CWI observables (θ, Kd) and the global crack length (Eqs. (3) and (4)) are thus validated for a multiple scattering medium as well as for a reverberating medium. The scattering events mainly occur at the reflection with the medium boundaries in the reverberating case: the scattering mean free path is therefore larger than in the previous case of multiple scattering by distributed heterogeneities. As a consequence, and considering that the same time window is analyzed in each case, the CWI observable values are smaller in the reverberating case. The addition of disorder improves the sensitivity of the method. Overall, the proposed method is rather robust to the medium configuration, be it a homogeneous reverberating material or a heterogeneous material.

5. Conclusion

In this paper, 2D SEM was used to perform a parametric sensitivity study of NCWI in a multiple-scattering medium with a localized microcracked zone. Parametric studies between the CWI observables, *i.e.* the

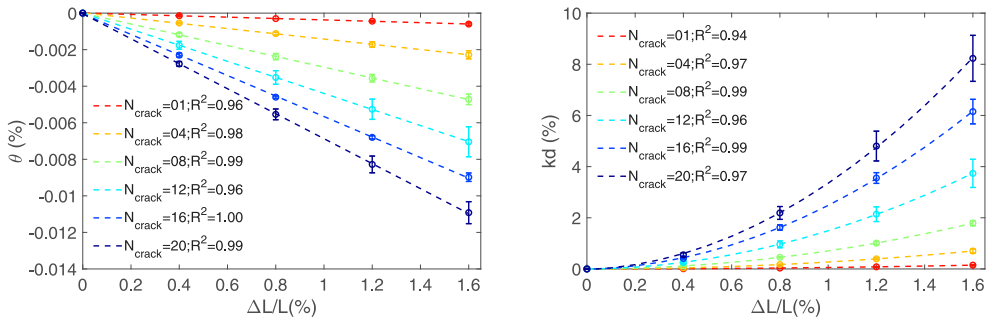

(a) (b)

Fig. 6. CWI observables versus changes in crack length ($\Delta L_{crack}/L_{crack}$) for the reverberating medium. For each fixed number of random cracks ($N_{crack} \in [1, 4, 8, 12, 16, 20]$), six numerical models were used: (a) Relative variation in velocity θ_{coda} versus $\Delta L_{crack}/L_{crack}$; (b) Remnant decorrelation coefficient Kd versus $\Delta L_{crack}/L_{crack}$..

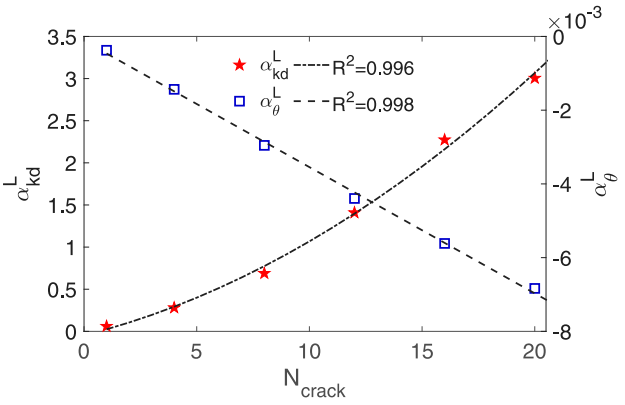

Fig. 7. Slopes of CWI observables with crack length changes in terms of the crack density N_{crack} for the reverberating medium. For each fixed number of random cracks ($N_{crack} \in [1, 4, 8, 12, 16, 20]$), five numerical models were used. For each group of models, five crack disorder arrangements were considered in order to calculate the mean value of α^L_{θ} (red pentagram) and α^L_{θ} (blue square). Their slopes versus crack density N_{crack} are obtained with linear and quadratic regression and illustrated with dash–dot line and dashed line, respectively.

relative variation in velocity θ_{coda} and the remnant decorrelation coefficient Kd, and effective variations in crack length in different samples were performed numerically. The crack length average variations were assumed to be the consequence of different levels of pump waves of high amplitude, enabling the simulation of the probe wave propagation only. The results show that θ_{coda} is linearly proportional to the sum of the changes in crack length and Kd was found to be proportional to the square of the sum of changes in crack length. This dependence has also been observed in a previous numerical study [46] and in the experiments reported by Zhang et al. [42]. Our results also confirm the sensitivity of the NCWI method to tiny changes in the tested material, this is a step towards a more quantitative evaluation of damage in complex solids by ultrasonic waves.

Comparing to our previously reported model [46], which allows interpretations of NCWI results from a macroscopic point of view under effective-medium approximation, the model reported herein describes the nonlinear phenomenon from a more microscopic point of view: the NCWI observation is related to a change in the effective crack length. With such a model bridging the gap between macroscopic observation (i.e. NCWI results) and microscopic characteristics of the propagation medium (i.e. cracks density and length), the obtained simulation results contribute to a deeper understanding of the NCWI method in a multi-scattering medium, as well as in a reverberating medium with the presence of microcracks.

Indeed, the reported model cannot describe the nonlinear phenomenon fully since the dynamic response of cracks' interfaces to the pump wave excitation is omitted. However, the authors believe, by avoiding such a computational conundrum that involves the wave motion problem and the dynamic contact problem simultaneously, this simplified model would allow a more fundamental yet intuitive understanding of the nonlinear acoustic effect. Since the NCWI observables are quantitatively related to the change in crack's effective length, our future research aims to take into account the relationship between the pump wave and crack length to establish a fully quantitative damage assessment approach and to extend its application scope beyond the pumping effect.

Declaration of competing interest

The authors declare that they have no known competing financial interests or personal relationships that could have appeared to influence the work reported in this paper.

Acknowledgments

This research was supported by the RFI LMAc (Recherche Formation Innovation Le Mans Acoustique), funded by the Région Pays-de-la-Loire (France). The authors appreciate the support from the Key laboratory grant (JCKYS2019604SSJS010) and are particularly grateful to Yann Capdeville for support in applying the numerical method.

References

[1] R.A. Guyer, P.A. Johnson, Nonlinear mesoscopic elasticity: Evidence for a new class of materials, Phys. Today 52 (4) (1999) 30–36.
[2] J.A. Ten Cate, Slow dynamics of earth materials: An experimental overview, Pure Appl. Geophys. 168 (12) (2011) 2211–2219.
[3] P. Lundqvist, N. Rydén, Acoustoelastic effects on the resonance frequencies of prestressed concrete beams—Short-term measurements, NDT & E Int. 50 (2012) 36–41.
[4] J.N. Eiras, J.S. Popovics, M.V. Borrachero, J. Monzó, J. Payá, The effects of moisture and micro-structural modifications in drying mortars on vibration-based NDT methods, Constr. Build. Mater. 94 (2015) 565–571.
[5] P. Blanloeuil, L.R.F. Rose, J.A. Guinto, M. Veidt, C.H. Wang, Closed crack imaging using time reversal method based on fundamental and second harmonic scattering, Wave Motion 66 (2016) 156–176.
[6] P.A. Johnson, A. Sutin, Slow dynamics and anomalous nonlinear fast dynamics in diverse solids, J. Acoust. Soc. Am. 117 (2005) 124.
[7] D. Pasqualini, K. Heitmann, J.A. Ten Cate, S. Habib, D. Higdon, P.A. Johnson, Nonequilibrium and nonlinear dynamics in berea and fontainebleau sandstones: low-strain regime, J. Geophys. Res. 112 (B1) (2007) B01204.
[8] G. Renaud, S. Callé, J. Remenieras, M. Defontaine, Exploration of trabecular bone nonlinear elasticity using time of flight modulation, IEEE Trans. Ultrason. Ferroelectr. Freq. Control 55 (7) (2008) 1–10.
[9] S. Callé, H. Moreschi, G. Renaud, M. Defontaine, Ultrasound propagation in trabecular bone: a numerical study of the influence of microcraks, Ultrasonics 54 (5) (2014) 1231–1236.
[10] V. Tournat, V.E. Gusev, B. Castagnède, Subharmonics and noise excitation in transmission of acoustic wave through unconsolidated granular medium, Phys. Lett. A 326 (5–6) (2004) 340–348.
[11] V. Tournat, V.Y. Zaitsev, V.E. Gusev, V.E. Nazarov, P. Béquin, B. Castagnède, Probing weak forces in granular media through nonlinear dynamic dilatancy: clapping contacts and polarization anisotropy, Phys. Rev. Lett. 92 (8) (2004) 085502.
[12] V. Tournat, V. Gusev, Nonlinear effects for coda-type elastic waves in stressed granular media, Phys. Rev. E 80 (2009) 011306.
[13] K. Wang, M. Liu, Z. Su, S. Yu, Z. Fan, Analytical insight into breathing crack-induced acoustic nonlinearity with an application to quantitative evaluation of contact cracks, Ultrasonics 88 (2018) 156–157.
[14] R. Radecki, Z. Su, L. Cheng, P. Packo, W.J. Staszewski, Modelling nonlinearity of guided ultrasonic waves in fatigued materials using a nonlinear local interaction simulation approach and a spring model, Ultrasonics 84 (2018) 272–289.
[15] K.R. McCall, R. Guyer, Equation of state and wave propagation in hysteretic nonlinear elastic materials, J. Geophys. Res. B Solid Earth 99 (B12) (1994) 23887–23897.
[16] A. Moussatov, V. Gusev, B. Castagnéde, Self-induced hysteresis for nonlinear acoustic waves in cracked material, Phys. Rev. Lett. 90 (12) (2003) 124301–124305.
[17] V.E. Nazarov, A.V. Radostin, L.A. Ostrovsky, I.A. Soustova, Wave processes in media with hysteretic nonlinearity. Part I, Acoust. Phys. 49 (2003) 344–353.
[18] J. Cabaret, P. Béquin, G. Theocharis, V. Andreev, V.E. Gusev, V. Tournat, Nonlinear hysteretic torsional waves, Phys. Rev. Lett. 115 (2015) 054301.
[19] V.Y. Zaitsev, V.E. Gusev, B. Castagnède, Thermoelastic mechanism for logarithmic slow dynamics and memory in elastic wave interaction with individual cracks, Phys. Rev. Lett. 90 (7) (2003) 075501–1–4.
[20] J.A. Ten Cate, D. Pasqualini, S. Habib, K. Heitmann, D. Higdon, P.A. Johnson, Nonlinear and nonequilibrium dynamics in geomaterials, Phys. Rev. Lett. (93) (2004) 065501–065504.
[21] G.A. Gist, Fluid effects on velocity and attenuation in sandstones, J. Acoust. Soc. Am. 96 (1994) 1158–1173.
[22] P.A. Johnson, B. Zinszner, P.N.J. Rasolofosaon, Resonance and elastic nonlinear phenomena in rock, J. Geophys. Res. B Solid Earth 101 (B5) (1996) 11553–11564.
[23] P.A. Johnson, R.A. Guyer, The astonishing case of mesoscopic elastic nonlinearity, Phys. Today.
[24] V. Zaitsev, Nonlinear acoustics in studies of structural features of materials, MRS Bull. 44 (5) (2019) 350–360.
[25] D. Donskoy, A. Sutin, A. Ekimov, Nonlinear acoustic interaction on contact interfaces and its use for nondestructive testing, NDT & E Int. 34 (4) (2001) 231–238.

[26] J.-Y. Kim, L.J. Jacobs, J. Qu, J.W. Littles, Experimental characterization of fatigue damage in a nickel-base superalloy using nonlinear ultrasonic waves, J. Acoust. Soc. Am. 120 (3) (2006) 1266–1273.
[27] K. Van Den Abeele, A. Sutin, J. Carmeliet, P.A. Johnson, Micro-damage diagnostics using nonlinear elastic wave spectroscopy (NEWS), NDT & E Int. 34 (4) (2001) 239–248.
[28] S. Haupert, G. Renaud, J. Rivière, M. Talmant, P.A. Johnson, P. Laugier, High-accuracy acoustic detection of nonclassical component of material nonlinearity, J. Acoust. Soc. Am. 130 (5) (2011) 2654–2661.
[29] G. Renaud, J. Rivière, P.-Y.L. Bas, P.A. Johnson, Hysteretic nonlinear elasticity of berea sandstone at low-vibrational strain revealed by dynamic acousto-elastic testing, Geophys. Res. Lett. 40 (4) (2013) 715–719.
[30] J. Rivière, G. Renaud, R. Guyer, P.A. Johnson, Pump and probe waves in dynamic acousto-elasticity: Comprehensive description and comparison with nonlinear elastic theories, J. Appl. Phys. 114 (5) (2013) 089903.
[31] J. Rivière, M.C. Remillieux, Y. Ohara, B.E. Anderson, S. Haupert, T.J. Ulrich, P.A. Johnson, Dynamic acousto-elasticity in a fatigue-cracked sample, J. Nondestruct. Eval. 33 (2) (2014) 216–225.
[32] J.N. Eiras, Q.A. Vu, M. Lott, J. Payá, V. Garnier, C. Payan, Dynamic acousto-elastic test using continuous probe wave and transient vibration to investigate material nonlinearity, Ultrasonics 69 (2016) 29–37.
[33] R.A. Guyer, P.A. Johnson, Nonlinear Mesoscopic Elasticity, Wiley-VCH, 2009.
[34] O. Buck, W.L. Morris, J.M. Richardson, Acoustic harmonic generation at unbonded interfaces and fatigue cracks, Appl. Phys. Lett. 33 (5) (1978) 371–373.
[35] G. Poupinet, W.L. Ellsworth, J. Fréchet, Monitoring velocity variations in the crust using earthquake doublets : an application to the Calaveras fault, California, J. Geophys. Res. 89 (1984) 5719–5731.
[36] R. Snieder, A. Grêt, H. Douma, J. Scales, Coda wave interferometry for estimating nonlinear behavior in seismic velocity, Science 295 (5563) (2002) 2253–2255.
[37] E. Larose, S. Hall, Monitoring stress related velocity variation in concrete with a 2×10^{-5} relative resolution using diffuse ultrasound, J. Acoust. Soc. Am. 125 (4) (2009) 1853–1856.
[38] T. Planès, E. Larose, A review of ultrasonic coda wave interferometry in concrete, Cem. Concr. Res. 53 (2013) 248–255.
[39] R.L. Weaver, C. Hadziioannou, E. Larose, M. Campillo, On the precision of noise correlation interferometry, Geophys. J. Int. 185 (3) (2011) 1384–1392.
[40] A. Bassil, X. Wang, X. Chapeleau, E. Niederleithinger, O. Abraham, D. Leduc, Distributed fiber optics sensing and coda wave interferometry techniques for damage monitoring in concrete structures, Sensors 19 (2) (2019) 356.
[41] E. Niederleithinger, X. Wang, M. Herbrand, M. Müller, Processing ultrasonic data by coda wave interferometry to monitor load tests of concrete beams, Sensors 18 (6) (2018) 1971.
[42] Y. Zhang, V. Tournat, O. Abraham, O. Durand, S. Letourneur, A.L. Duff, B. Lascoup, Nonlinear mixing of ultrasonic coda waves with lower frequency-swept pump waves for a global detection of defects in multiple scattering media, J. Appl. Phys. 113 (6) (2013) 064905.
[43] B. Hilloulin, Y. Zhang, O. Abraham, A. Loukili, F. Grondin, O. Durand, V. Tournat, Small crack detection in cementitious materials using nonlinear coda wave modulation, NDT & E Int. 68 (2014) 98–104.
[44] J.B. Legland, O. Abraham, G. Villain, O. Durand, V. Tournat, Suivi du gradient de teneur en eau dans les bétons par modulation non linéaire de la coda ultrasonore, Congés français d'acoustique, Le Mans.
[45] D. Komatitsch, J.P. Vilotte, The spectral element method: an effective tool to simulate the seismic response of 2D and 3D geological structures, Bull. Seismol. Soc. Am. 88 (1998) 5961–5972.
[46] D. Chen, J.-B. Pageot, G. Legland, O. Abraham, M. Chekroun, V. Tournat, Numerical modeling of ultrasonic coda wave interferometry in a multiple scattering medium with a localized nonlinear defect, Wave Motion 72 (2017) 228–243.
[47] G. Chen, D. Pageot, O. Abraham, Y. Zhang, M. Chekroun, V. Tournat, Nonlinear coda wave interferometry: Sensitivity to wave-induced material property changes analyzed via numerical simulations in 2D, Ultrasonics 99 (2019) 105968.
[48] F. Xie, E. Larose, L. Margerin, Y. Zhang, T. Planès, Characterizing extended changes in multiple scattering media using coda wave decorrelation: numerical simulations, Waves Random Complex Media 28 (2018) 1–14.
[49] G.M. Mavko, A. Nur, Effect of non-elliptical cracks on compressibility of rocks, J. Geophys. Res. 83 (9) (1978) 4459–4468.
[50] C. Geuzaine, J.-F. Remacle, GMSH: a three-dimensional finite element mesh generator with built-in pre- and post-processing facilities, Internat. J. Numer. Methods Engrg. 79 (11) (2009) 1309–1331.
[51] Y. Zhang, V. Tournat, O. Abraham, O. Durand, S. Letourneur, A.L. Duff, B. Lascoup, Nonlinear modulation of ultrasonic coda waves for the global evaluation of damage levels in complex solids, Ultrasonics 73 (2016) 245–252.
[52] F. Xie, W. Li, Y. Zhang, Monitoring of environmental loading effect on the steel with different plastic deformation by diffuse ultrasound, Struct. Health Monit. 18 (2) (2019) 602–609.
[53] K. Wang, W. Cao, L. Xu, X. Yang, Z. Su, X. Zhang, L. Chen, Diffuse ultrasonic wave-based structural health monitoring for railway turnouts, Ultrasonics 101 (2020) 106031.
[54] Y. Zhang, E. Larose, L. Moreau, G. d'Ozouville, Three-dimensional in-situ imaging of cracks in concrete using diffuse ultrasound, Struct. Health Monit. 17 (2) (2018) 279–284.
[55] E. Larose, Mesoscopic of ultrasound and seismic waves: application to passive imaging, 31, 2006, EDZ Sciences.
[56] D. Gross, C. Zhang, Wave propagation in damaged solids, Int. J. Solids Struct. 29 (14) (1992) 1763–1779.